Asia-Pac. J. Atmos. Sci., 51(2), 137-155, 2015
DOI:10.1007/s13143-015-0064-7
pISSN 1976-7633 / eISSN 1976-7951

# Simulation of Impact from Stratospheric Ozone on Global Tropospheric Ozone Distribution with a Chemistry Transport Model: A Case Study during the 1990-1991 Period

**Kuo-Ying Wang[1] and Wen-Shung Kau[2]**

[1]*Department of Atmospheric Sciences, National Central University, Chung-Li, Taiwan*
[2]*Department of Atmospheric Sciences, National Taiwan University, Taipei, Taiwan*

(Manuscript received 11 July 2014; accepted 22 February 2015)


**Abstract:** In this work we examine the effect of ozone ($O_3$) from the stratosphere on the $O_3$ levels in the troposphere. The tropopause is defined according to the potential vorticity (PV) and potential temperature distribution. Annual simulations were performed with and without stratospheric $O_3$ in the model to access the impact of stratospheric $O_3$ on tropospheric $O_3$ distribution. Our results show that surface $O_3$ over the tropical marine boundary layer is dominated by in-situ photochemistry in the troposphere. The maintenance of the inter-hemispheric asymmetry in ozone over the extra-tropical marine boundary layer is dominated by the transport of $O_3$ from the stratosphere. Comparisons between the model and the surface measurements show that the model without stratospheric $O_3$ exhibits a hemispheric summer maximum, emphasizing the contributions of transport of $O_3$ and $O_3$ producing precursors from continental regions during the summer months, whilst no clear spring $O_3$ maximum is found. About 50%-80% of $O_3$ in the lower troposphere over the northern hemisphere mid-latitudes are photochemically produced during the northern hemisphere summer. About 20%-40% is due to tropospheric photochemistry in the lower troposphere during the northern hemisphere spring. We conclude that $O_3$ transported from the stratosphere is the dominating factor for the spring $O_3$ maximum over the extra-tropical latitudes, while the photochemical ozone production is the dominating factor for $O_3$ over the tropical marine boundary layer environments and over the land surface emission areas.

**Key words:** Ozone, chemistry transport model, spring ozone maximum, inter-hemispheric asymmetry, stratosphere

## 1. Introduction

Given the significant impact ozone can have on the tropospheric radiation budget, the tropospheric oxidizing capacity, and future ground-level air pollution and human health under climate change (e.g., Künzli et al., 2000), understanding the processes controlling $O_3$ levels in the troposphere is of great importance (Park and Kim, 2014).

There are essentially two views regarding the processes regulating the concentrations of $O_3$ in the troposphere (e.g., Monks, 2000). The first view is that transport from the stratosphere to the troposphere is the dominating source of $O_3$ in the troposphere (e.g., Moody et al., 1995; Oltmans et al., 1996; see also Monks, 2000, and references therein). The second view is that the photochemical oxidation of carbon monoxide (CO) and hydrocarbons,in the presence of nitrogen oxides (NOx), is the dominating source of $O_3$ in the troposphere (e.g., Jacob et al., 1996; Wang et al., 1998; see also Monks, 2000, and references therein).

An approach employed to access the impact of the stratospheric $O_3$ on the levels of $O_3$ in the troposphere is by using a specified stratospheric $O_3$ tracer (e.g., Roelofs and Lelieveld, 1997; Roelofs et al., 1997; Wang et al., 1998; Lelieveld and Dentener, 2000). In this approach, the stratospheric $O_3$ tracer is transported from the stratosphere into the troposphere following dynamical processes in the upper troposphere and lower stratosphere region (e.g., Holton et al., 1995). Once the stratospheric $O_3$ tracer is in the troposphere, it is subjected to the photochemical reactions that destroy $O_3$, i.e., reactions with hydroxyl radical (OH) and hydrogen dioxide ($HO_2$), and through $O_3$ photodissociation followed by reaction with water vapor ($H_2O$) to produce OH in the troposphere. There is no photochemical $O_3$ production for this stratospheric $O_3$ tracer. The stratospheric $O_3$ tracer is also subjected to removal by dry deposition at the surface. Hence, the difference between the concentration of $O_3$ calculated using the full tropospheric chemistry model, and the concentration of the stratospheric $O_3$ tracer in the troposphere is a measure of $O_3$ in the troposphere that originates from photochemistry in the troposphere (Roelofs et al., 1997).

Based on this approach, Roelofs et al. (1997) calculated a stratospheric $O_3$ contribution of about 40% of $O_3$ in the troposphere. Roelofs and Lelieveld (1997) concluded that $O_3$ from the stratosphere contributes significantly to surface $O_3$ in winter and spring, while in summer the surface $O_3$ is largely determined by photochemical production. Wang et al. (1998) concluded that stratospheric $O_3$ contributes about 30% of $O_3$ in the troposphere at mid-latitudes in winter, 10% in summer, and 5% in tropics.

In this work we use an alternative way for studying the impact of stratospheric $O_3$ on the levels of $O_3$ in the troposphere with a three-dimensional (3D) global chemistry transport model

Corresponding Author: Kuo-Ying Wang, Department of Atmospheric Sciences, National Central University, Chung-Li, Taiwan.
E-mail: kuoying@mail.atm.ncu.edu.tw

(CTM). Instead of using a stratospheric $O_3$ tracer, we assume that there is no stratospheric $O_3$ in the model. Hence, the spatial and temporal variations of $O_3$ in the troposphere is entirely due to tropospheric photochemistry production. The results from this no stratospheric $O_3$ simulation is compared with the results from simulation where stratospheric $O_3$ is included to access the importance of stratospheric $O_3$ in the troposphere. Notice that zero $O_3$ in the stratosphere only rules out downward $O_3$ fluxes from the stratosphere into the troposphere. The upward $O_3$ fluxes from the troposphere into the stratosphere still working in the simulation results shown in this work.

We note that the meteorological data selected for this work were taken from the period 1990-1991, a period with moderate El Niño effect (Tourre and White, 2005), hence the results shown in this work represents a period exhibiting higher air mass fluxes during the stratosphere-troposphere exchange (STE) processes in the upper troposphere and lower stratosphere (UTLS) region than other non-El Niño years. The difference of STE $O_3$ fluxes between an El Niño year and the non-El Niño years in the tropospheric $O_3$ burden can be gleaned from a study covering the 1996-2000 period and including a strong 1997-1998 El Niño event. Voulgarakis et al. (2011) found that $O_3$ burden in 1998 is higher than the rest of non El Niño years; inter-annual variability of $O_3$ levels in the stratosphere has low impact on the variability of $O_3$ levels in the troposphere; and net chemical $O_3$ tendency during the 1998 El Niño year is lower than other years. As such, the high $O_3$ burden in the troposphere in 1998 is mainly controlled by the elevated STE $O_3$ fluxes during the El Niño period. This finding of high tropospheric $O_3$ burden in association with high STE process during the 1997-1998 period is also consistent with a study containing a longer period of 1990-2009 from Hess and Zbinden (2013), who also found strong $O_3$ burden in the troposphere associated with the 1998-1999 period. The El Niño/Southern Oscillation (ENSO) and the stratospheric Quasi-Biennial Oscillation (QBO) can contribute to 40% of interannual variations in the strength of the stratospheric circulation, and around 2% change of $O_3$ levels in the northern hemisphere mid-latitudes (Neu et al., 2014). Another estimate shows QBO contributes 20% of interannual STE variance in the norther hemisphere, and 40% in the southern hemisphere (Hsu and Prather, 2009).

In addition to a period with moderate El Niño effect, the radiative forcing from the presence of volcano aerosols during the eruption of Mount Pinatubo in June 1991 could act to enhance planetary wave activity, leading to further enhancement of meridional circulation (Schauffler and Daniel, 1994). Mount Pinatubo eruption also had occurred during the change of QBO from westerly to easterly flow at 50 hPa in the tropical lower stratosphere, indicating increase in planetary wave activity. Hence, the enhanced meridional circulation and enhanced planetary wave activity driven by the radiative forcing from Mount Pinatubo aerosols, combined with the easterly phase of the QBO could act in concert to increase circulation and wave activity (Schauffler and Daniel, 1994).

## 2. Methods

### *a. The IMS chemistry transport model*

A 3D tropospheric CTM called integrated modeling system (IMS) is used in this work (Wang et al., 2001a, b). The IMS CTM contains detailed gas-phase chemistry, including reaction mechanism for nitrogen oxides (NOx), methane ($CH_4$), non-methane hydrocarbons (NMHC), biogenic volatile organic compounds (VOCs), and some sulfur and halogen species (Wang et al., 2001b). Specified emissions for anthropogenic sources were taken from Emission Database for Global Atmospheric Research (EDGAR) and the Global Emission InitiAtive (GEIA) (Wang et al., 2001a). The geographical distribution of the sinks of important tropospheric species ($O_3$, nitrogen dioxide ($NO_2$), peroxyacetyl nitrate (PAN), carbon monoxide (CO), etc) are considered via the dry and wet deposition processes. Transport of long-lived species are achieved using the semi-Lagrangian method (Wang and Shallcross, 2000). Convective cloud transport of long-lived species are parameterized with a mass-flux convective scheme (Wang et al., 2001a). Mixing of chemical species in the atmospheric boundary layer is modeled with a non-local convective scheme (Wang et al., 1999).

The model is driven by the meteorological analysis data. Meteorological variables such as zonal wind, meridional wind, temperature, specific humidity, and surface pressure are used by the IMS CTM at fixed frequency for the entire simulation period. In this work we use 6-hourly analysis data obtained from the European Centre for Medium Range Weather Forecast (ECMWF). The model contains 19 layers in the vertical, extending from surface to about 10 hPa. The model has a horizontal resolution of 7.5° in longitude and 4.5° in latitude.

### *b. The control run*

In order to conduct the 3D simulations on a global domain with a complex global model such as the IMS CTM used in this work, the IMS codes have been developed since 1995 to make global chemistry simulation feasible. The IMS model was multitasked and run parallely on the shared-memory CRAY J90 at National Taiwan University (Wang et al., 2000). The model was run for two years with full tropospheric chemistry (Wang et al., 2001b). The results, composed from every 6-hour model output frequency, from the second year (1991) were used for the results shown in the work.

### *c. A tropospheric simulation without stratospheric $O_3$*

Since the aim of this work is to study the processes in the troposphere, the concentrations of $O_3$, reactive nitrogen (NOy), and nitric acid ($HNO_3$) in the stratosphere are prescribed similar to the method of Berntsen and Isaksen (1997). The stratospheric $O_3$ concentration is interpolated from the climatological ozone data used in the National Center for Atmospheric Research (NCAR) Community Climate Model 2

(CCM2) model (Hack et al., 1993). The definition of the tropopause is taken as: 1) the model potential vorticity unit (PVU) is 1.6 (1 PVU = $10^{-6} m^2 K s^{-1} kg^{-1}$), for latitudes pole-ward 25°; and 2) the potential temperature is 380 K, for latitudes between 25°N and 25°S (Hoskins, 1991).

In order to study the effect of stratospheric $O_3$ in the troposphere, we conduct a tropospheric simulation without stratospheric $O_3$. In this simulation, all $O_3$ concentrations in the stratosphere are set to zero (i.e., $O_3$ constantly removed from the stratosphere) during the course of an annual integration. Hence there is no influx of $O_3$ from the lower stratosphere into the troposphere. However, the model allows $O_3$ export to the lower stratosphere from the upper troposphere. The result from another experiment without any $O_3$ exchange between the lower stratosphere and the upper troposphere will be reported in a separate study. We note that the same clear sky photolysis rates look-up *J* table corrected by the presence of cloud effect (Wang et al., 2001b) during the model integration was used for simulations with and without stratospheric $O_3$ in the model.

### *d. Tropopause distribution*

In the model integration, each model box below the tropopause is said to be in the troposphere and is assigned to a number 1, while the model box above the tropopause is said to be in the stratosphere and is assigned to a number 0. Hence, a time-varying distribution of these 3D 0s and 1s in the upper troposphere and lower stratosphere (UTLS) associated with the wave activities is expected in the UTLS region (e.g., Holton et al., 1995, and references therein). A model box always has a

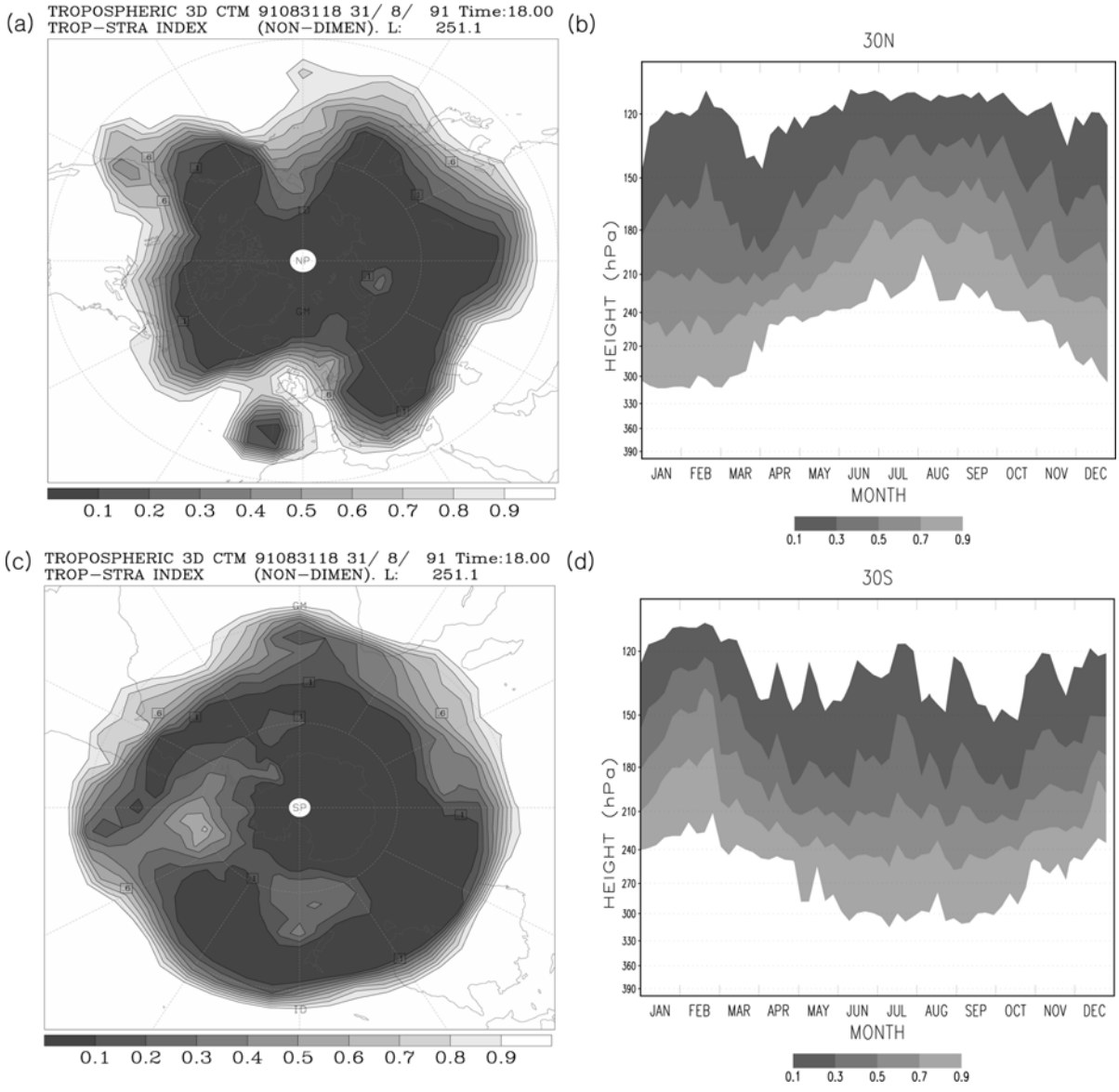


**Fig. 1.** Distribution of the tropopause calculated at 250 hPa in August for the northern hemisphere (upper left) and the southern hemisphere (upper right); time-height cross sections of the zonal mean tropopause at 30°N (lower left) and 30°S.

value of 1/0 if it stays permanently in the troposphere/stratosphere. However, if a model box is in the UTLS region, it is exposed to sharp transitions of air coming from either the lower stratosphere or the upper troposphere, and its assigned value will change swiftly between 1 and 0. The frequency of the switch between 1 and 0 depends entirely on the STE frequency (Elbern et al., 1998), while the depth (altitude) where a box with 1 or with 0 can appear rely on the strength and maintenance of the wave instability in the UTLS region. Hence, a time average of these 3D model boxes exhibits the distribution of boxes with values varying between 0 and 1 in the UTLS region.

The upper panel of Fig. 1 shows examples of average spatial distribution of the model tropopause occurrence in August (1991) for the northern hemisphere and the southern hemisphere, respectively. The wavy structure of the tropopause is clearly seen at about 250 hPa (~10 km in mid-latitude). At this altitude, the tropical regions are entirely in the troposphere, while most of the high latitudes in both hemispheres are entirely in the stratosphere. Areas with contour values varying between 0 and 1 indicate the exchange of air between the troposphere and the stratosphere (e.g., Vaughan et al., 1994; Holton et al., 1995; Bethan et al., 1996).

The lower panel of Fig. 1 shows a time-height cross-section of the zonal mean tropopause distribution at 30°N and 30°S, respectively. The change of the distribution of the tropopause occurrence between different seasons in each hemisphere is clearly seen for the extra-tropics pole-ward of about 30° (e.g., Elbern et al., 1998). For example, tropopause during the winter hemisphere is lower than during the summer hemisphere. A sharp transition of the tropopause, indicated by the values between 0 and 1, is concentrated at altitudes between 120 and 300 hPa for the winter and early spring, and at altitudes between 210 hPa and higher than 120 hPa for the summer months.

There are a couple of points to be highlighted here. Firstly, if the spring maximum of tropospheric ozone is associated with massive STE, it would have to be related to the depth of the events in spring rather than the STE frequency (Elbern et al., 1998) that would contribute to the ozone maximum (Monks, 2000). It is clear that the occurrence of the analyzed depth of the STE, indicated by the varying tropopause heights, is actually deeper during winter to early spring than during other seasons. Hence the analyses agree with Monks (2000). Secondly, a sharp transition in the tropopause height in the UTLS region indicates the need for a high resolution model to better resolve STE events and $O_3$ influx from lower stratosphere into the troposphere in this area (Logan, 1999). For example, Bethan et al. (1996) showed that the tropopause definition impacts greatly on the levels of $O_3$ in the troposphere.

### *e. Measuring effect of stratospheric $O_3$ in troposphere*

The effect of stratospheric $O_3$ on the levels of $O_3$ in the troposphere is examined by comparing the simulations with and without stratospheric $O_3$ in the model. The difference is measured by an $O_3$ ratio, which is the concentration of $O_3$ calculated without $O_3$ in the stratosphere to the concentration of $O_3$ calculated with $O_3$ in the stratosphere. The variations of this ratio indicate the effect of $O_3$ from the stratosphere in troposphere. For example, a ratio with unity indicating that stratospheric $O_3$ makes no impact at all. On the other hand, the small $O_3$ ratio indicates the big impact from the stratospheric $O_3$. We compare these two model simulations with surface and ozonesonde measurements. These comparisons aim at highlighting the spatial and temporal distribution of the impact of stratospheric $O_3$ in troposphere.

## 3. Results

### *a. Comparison with surface measurements*

Figure 2 compares time-series plots of modeled $O_3$ from calculations with and without stratospheric $O_3$, respectively, with observed $O_3$ levels at four sites located over the remote marine boundary layer. The model results calculated with stratospheric $O_3$ can reproduce the observed spring $O_3$ maximum at the surface, while the calculation without stratospheric $O_3$ shows no hemispheric spring maximum. The calculation without stratospheric $O_3$ shows much lower ozone level compared to the calculation with stratospheric ozone, and shows a summer maximum instead of the spring maximum indicating indicating the contributions of transport of $O_3$ and $O_3$ producing precursors from continental regions during the summer months. Particularly,the summer maximum at Westman Iceland in the northern hemisphere, and at Samoa in the southern hemisphere. We note that Bermuda shows an annual maximum from mid spring to late summer. The mid spring maximum at this site is likely to be associated with the transport of high $O_3$ and $O_3$ producing precursors from the North American continent (Moody et al., 1995).

### *b. Comparison with ozonesonde measurements*

While the previous surface comparisons show pronounced seasonal cycles and distinctive inter-hemispheric asymmetry in $O_3$ over the low latitude marine boundary layer, these comparisons were limited to the surface (e.g., Oltmans et al., 1996). Other factors such as free tropospheric $O_3$ and other $O_3$ precursor distribution, $O_3$ exchange in the upper troposphere and lower stratosphere, and atmospheric transport processes are crucial for understanding the chemical behavior over the remote marine troposphere.

(1) The Atlantic Ocean region

Figure 3 shows time-height cross sections of measured and modeled $O_3$ at North (Bermuda) and South (Ascension Island) Atlantic Ocean. For the North Atlantic site (Fig. 3a), elevated levels of $O_3$ extend from the upper troposphere to the middle and lower troposphere during the northern hemisphere spring

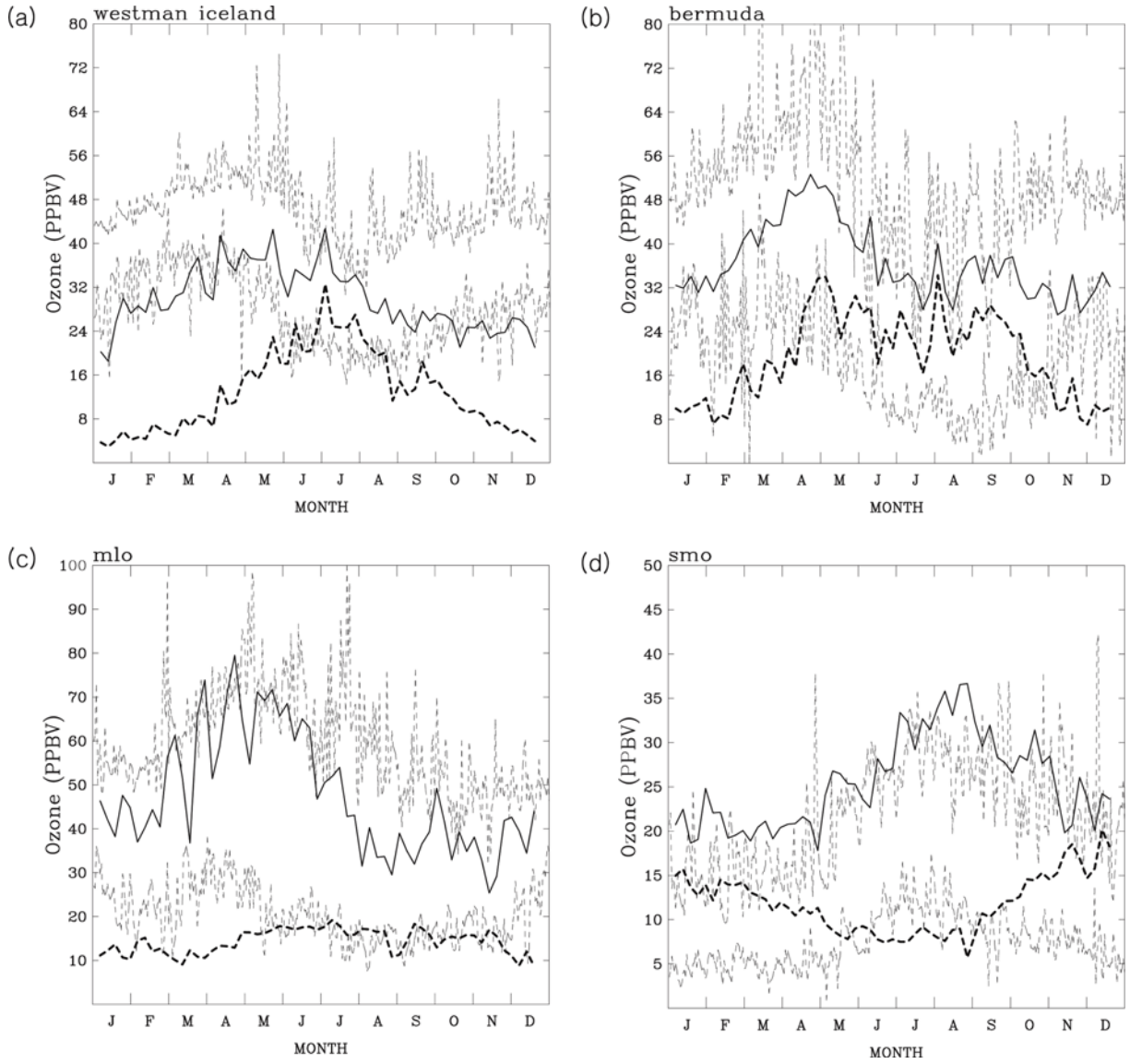


**Fig. 2.** Comparison of two modeled seasonal cycles of $O_3$ (ppbv) calculated with (solid thick lines) and without (bold dashed lines) stratospheric $O_3$ in the model at (a) Westman, Iceland (63.4°N, 20.3°W), (b) Bermuda 32°N, 65°W), (c) Mauna Loa (19.5°N, 155.6°W), and (d) Samoa (12.3°S, 170.6°W) with the measurements (thin dashed lines). Two measured $O_3$ levels (for the 1988-1992, except at Westman where the 1992-1997 data were used) are shown here, one for the daily maximum, while the other one for the daily minimum.

(March-May). High levels of $O_3$ are also seen in the lower stratosphere during this period. The modeled $O_3$ profiles at this location is shown in Fig. 3c. The observed high $O_3$ concentrations from the upper to the middle and lower troposphere during the northern hemisphere spring are generally well reproduced by the model. Both model and ozonesondes show a consistent and distinctive picture of the $O_3$ distribution in the troposphere during the northern hemisphere spring season compared with other seasons. High $O_3$ concentrations extend downward from the tropopause to near the surface, while low $O_3$ concentrations extend upward from the surface to near the tropopause. These characteristics are consistent with other analyses (Oltmans et al., 1996).

Moody et al. (1995) suggested that the elevated $O_3$ concentrations in the middle troposphere at this location during this period is associated with downward transport of $O_3$ from the upper and lower stratosphere. Based on the analyses of summer and spring ozonesondes at five locations over the North Atlantic, Oltmans et al. (1996) found the connection between high $O_3$ mixing rations and dry air in the middle and upper troposphere with large $O_3$ values in the tropopause region. They suggested that the stratosphere plays a major role in loading the troposphere with $O_3$, and high $O_3$ events usually extend downward from the tropopause region. From trajectory analyses showing the history of transport path, Oltmans et al. (1996) concluded that the upper troposphere and lower strato-

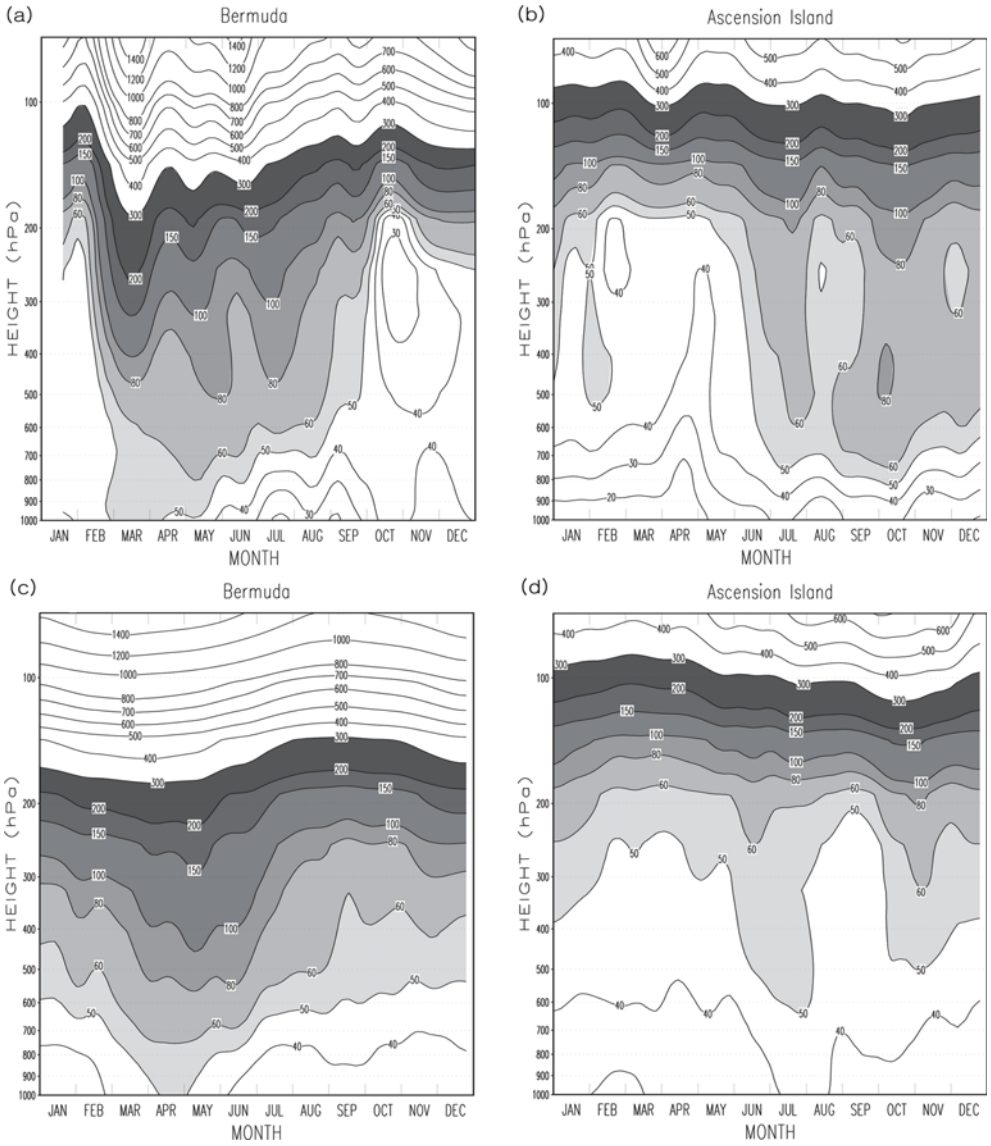


**Fig. 3.** Time-height cross sections of $O_3$ (ppbv) from measurements at Bermuda (32°N, 65°W) (a) and Ascension Island 8°S, 14°W) (b). The model calculation for these locations are shown in (c) and (d), respectively.

sphere was the source of elevated $O_3$ in the troposphere.

For the South Atlantic site (Fig. 3b), high $O_3$ concentrations are seen in the troposphere during the southern hemisphere spring season (September-November). High $O_3$ levels extend from the upper troposphere downward to near the surface during this season. Model calculations (Fig. 3d) at this South Atlantic site show similar spring $O_3$ maxima extending from the upper troposphere downward. These modeled results are in accordance with the measurements, though the modeled high $O_3$ levels in the upper troposphere do not extend as far downward as those shown in the measurements.

The enhanced tropospheric $O_3$ observed at Ascension Island during the July-October period is linked to dry season biomass burning (Diab et al., 1996). During September-October, gases from extensive fires in Brazil were transported by convective storms into the upper troposphere where tropospheric $O_3$ was photochemically produced and advected eastward over the southern Atlantic Ocean. The widespread fires in the deep convection-free central Africa were advected at low altitudes over the Atlantic Ocean (Browell et al., 1996; Jacob et al., 1996; Thompson et al., 1996). The modeled $O_3$ concentrations in the troposphere are lower than the ozonesonde measurements, indicate that biomass burning emissions in the model over the equatorial South America and central Africa regions are too low during the biomass burning season. Persistent and widespread $O_3$ maxima were observed and modeled during the hemispheric spring season (from March to May for the northern hemisphere; and from September to November for the southern hemisphere) than any other seasons of the year.

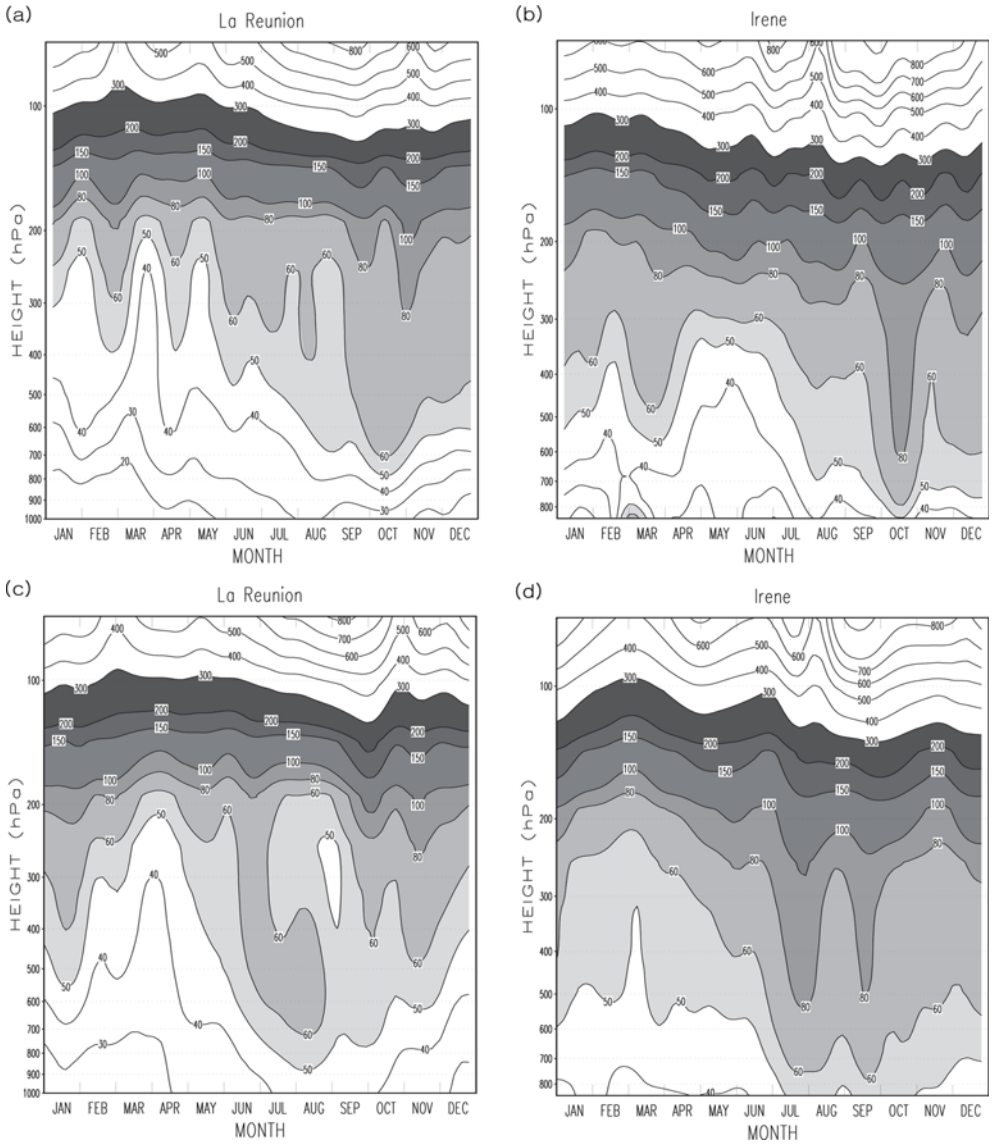


**Fig. 4.** Time-height cross sections of $O_3$ (ppbv) from measurements at La Reunion (21°S, 56°E) (a) and Irene (26°S, 28°E) (b). The model calculations for these locations are shown in (c) and (d), respectively.

(2) Western Indian Ocean region

Figure 4 shows comparisons of $O_3$ profiles from ozonesondes with model calculations at two locations over the Indian Ocean in the western southern hemisphere. Extensive high $O_3$ concentrations from the upper to lower troposphere are seen at these sites. Model calculations show similar southern hemisphere spring maxima in the troposphere comparable with the measurements. Both locations experienced the same sources for the elevated spring $O_3$ in the troposphere as to the southern hemisphere Atlantic sites of Ascension Island and Natal (Baldy et al., 1996; Diab et al., 1996). Analysis of one-year ozonesondes at Reunion Island (Fig. 4a) shows high levels of $O_3$ are observed from the upper to lower troposphere during the southern hemisphere spring (September-November). Baldy et al. (1996) reported that the elevated $O_3$ in the free troposphere during this period of time at this island is concomitant with active biomass burning in the southeastern African continent and Madagascar. Thompson et al. (1996) reported that features of elevated tropospheric $O_3$ (≥ 90 ppbv) extend in a band from 0° to 25°S, over the Indian Ocean, Africa, the Atlantic Ocean, and eastern South America during September-October. They showed a strong connection between regions of high $O_3$ and concentrated biomass burning.

(3) Western Pacific Ocean region

The observations and our previous modeling at sites over the South Atlantic Ocean showed that large-scale biomass burning emissions provide sources of elevated $O_3$ over the tropical South Atlantic Ocean. Long-range transport of biomass burning pollution could affect $O_3$ on a hemispheric scale (Fishman et

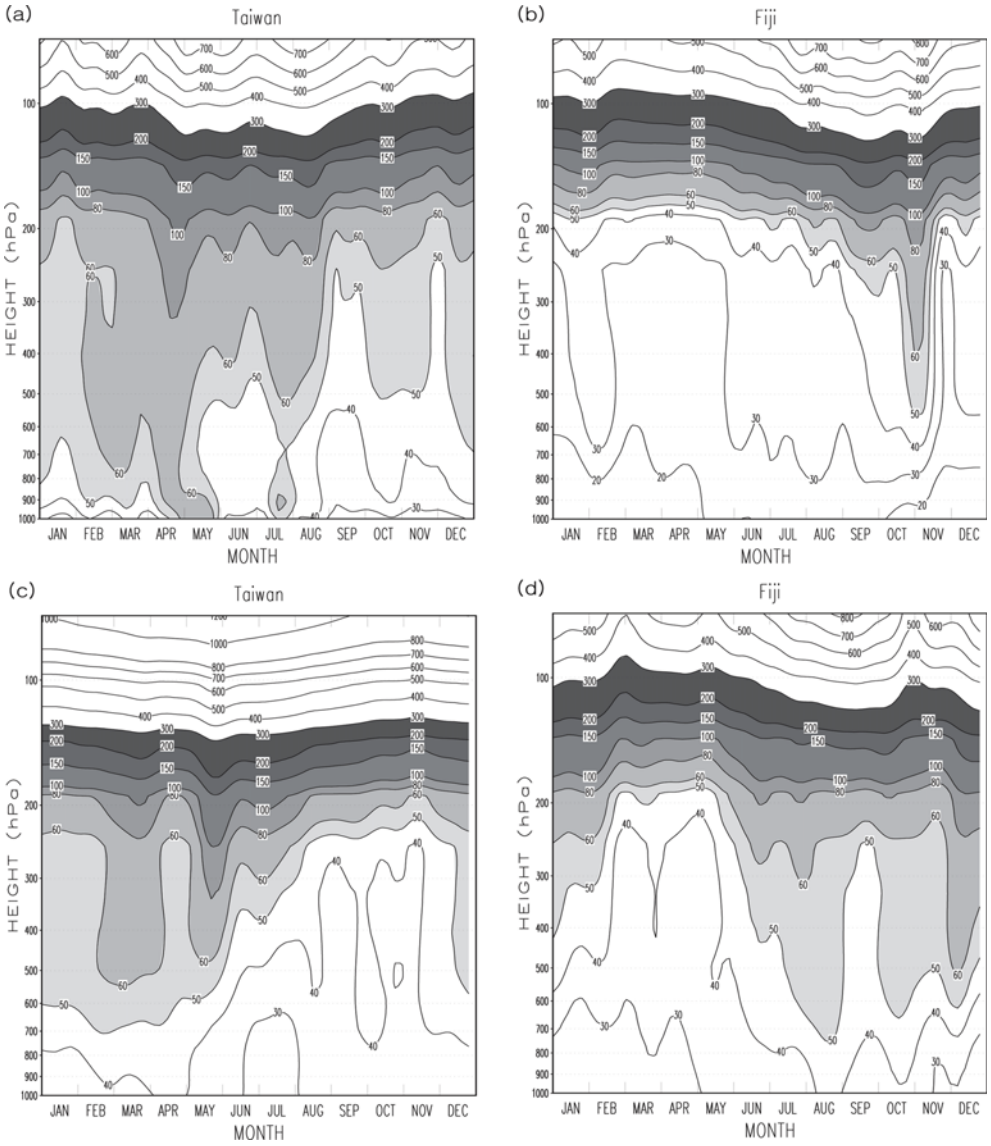


**Fig. 5.** Time-height cross sections of $O_3$ (ppbv) from measurements at Taiwan (25°N, 121°E) (a) and Fiji (17°S, 179°E) (b). The model calculations for these locations are shown in (c) and (d), respectively.

al., 1991; Schultz et al., 1999). Here we examine the extent of seasonal biomass burning influences over the Pacific Ocean. Figure 5 shows time-height cross sections of vertical profiles form ozonesondes and model calculations at Taiwan (in the subtropical western North Pacific Ocean), and Fiji (in the subtropical western South Pacific Ocean).

Observed $O_3$ profiles at Taiwan shows familiar spring $O_3$ maxima in the troposphere as to the sites in the North Atlantic Ocean. The model also shows a similar spring $O_3$ maximum, though the elevated $O_3$ concentrations do not extend as far down to near the surface as in the measurements. The major differences at altitudes below 4 km (~600 hPa) coincide with the altitude range most influenced by continental outflow (e.g., Crawford et al., 1997; Kajii et al., 1997). This indicates that the model underestimates the impact of continental outflow of $O_3$ precursors such as NO and NMHC (Crawford et al., 1997).

The observed and modeled $O_3$ profiles at Fiji show that elevated tropospheric $O_3$ occurs during the May-December period. Schultz et al. (1999) reported the importance of biomass burning emissions in South America and Africa for the $O_3$ budget at higher altitudes, and the NOx decomposed from transported PAN at altitudes below 4 km over the tropical South Pacific. This indicates that the model is able to produce the effect from biomass burning emissions and the long-range transport of ozone and ozone precursors to these sites.

(4) Central to eastern Pacific region

The South Pacific Ocean is the region of the tropical troposphere most remote from human activity (Schultz et al., 1999). Figure 6 shows $O_3$ vertical profiles from ozonesondes at

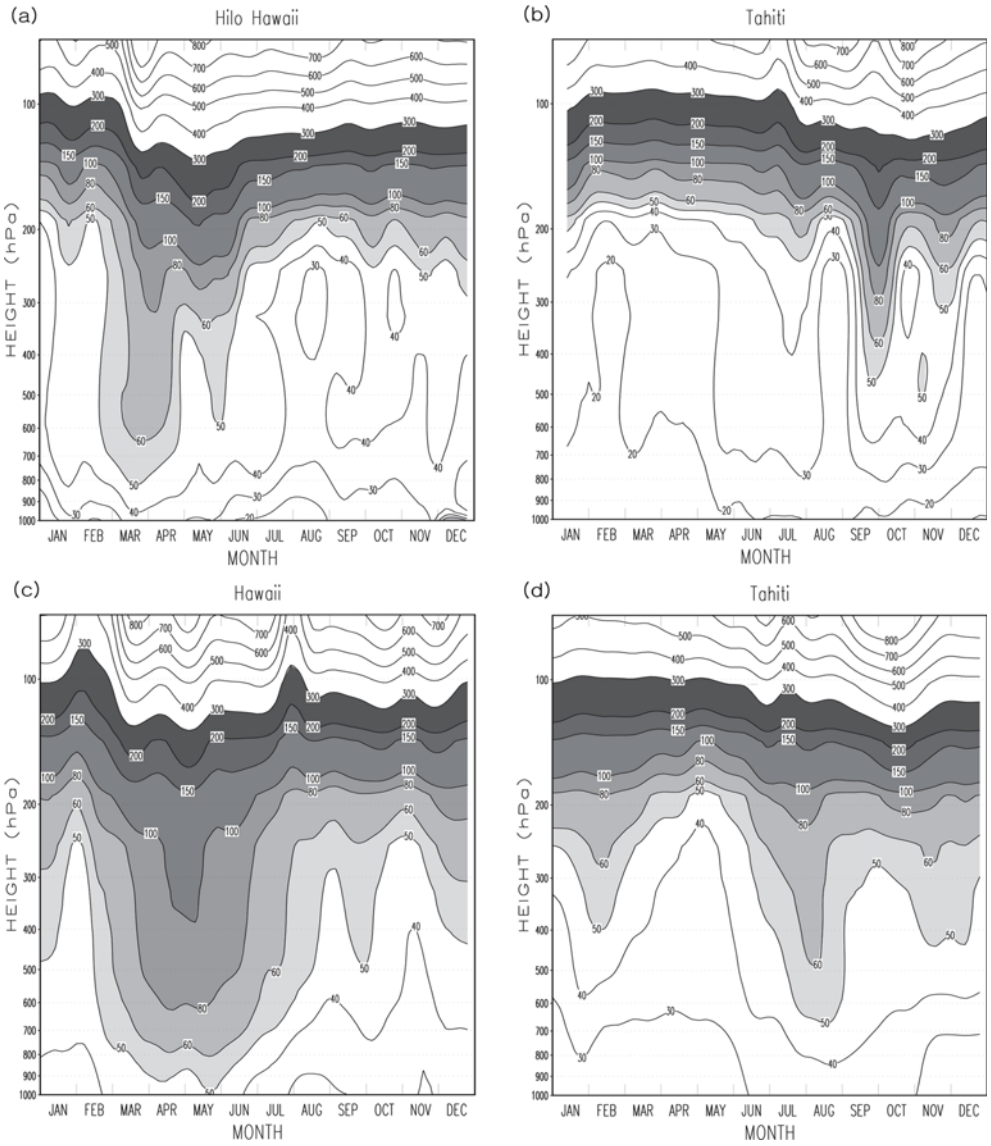


**Fig. 6.** Time-height cross sections of $O_3$ (ppbv) from measurements at Hawaii (20°N, 155°W) (a) and Tahiti (18°S, 149°W) (b). The model calculation for these locations are shown in (c) and (d), respectively.

Tahiti. At this location, an identifiable southern hemisphere spring $O_3$ maxima are seen as elevated $O_3$ concentrations extend from upper troposphere downward to the middle troposphere. The timing of this $O_3$ maxima, from September to November, coinciding with the intensive southern hemisphere biomass burning activities take place in South America, Africa, southeast Asia, and Oceania regions (Schultz et al., 1999).

The measurements also exhibit another period of elevated $O_3$ ($\geq 40$ ppbv) in the upper troposphere during the June-July period. The model calculations show that elevated $O_3$ extends from the upper to the middle troposphere at this period, indicating the contribution of biomass burning emissions. However, the model does not show the elevated $O_3$ observed in September-October. Modeled $O_3$ profiles at this South Pacific sites are also higher than the observations during June-August, indicating that the model contains too much local biomass burning emissions, or too much biomass burning is transported into this area from Africa or South America.

For the northern hemisphere site of Hawaii, both observed and modeled $O_3$ profiles show distinctive spring maximum. Elevated $O_3$ extend from upper troposphere to near the surface. Seasonal minima appear during the summer months. Wang et al. (1998) attributed this strong spring maximum to the long-range transport of Asian pollution over the northern Pacific Ocean atmosphere. Analyses of anthropogenic aerosols (Perry et al., 1999) and CO (Jaffe et al., 1997) at this site also shows a seasonal maximum in spring with sources from Asia continent (Perry et al., 1999).

The comparisons of time series $O_3$ vertical distribution over the Pacific Ocean basin shows inter-hemispheric asymmetry in $O_3$ concentrations between the northern hemisphere and the southern hemisphere subtropics. While the continental outflow

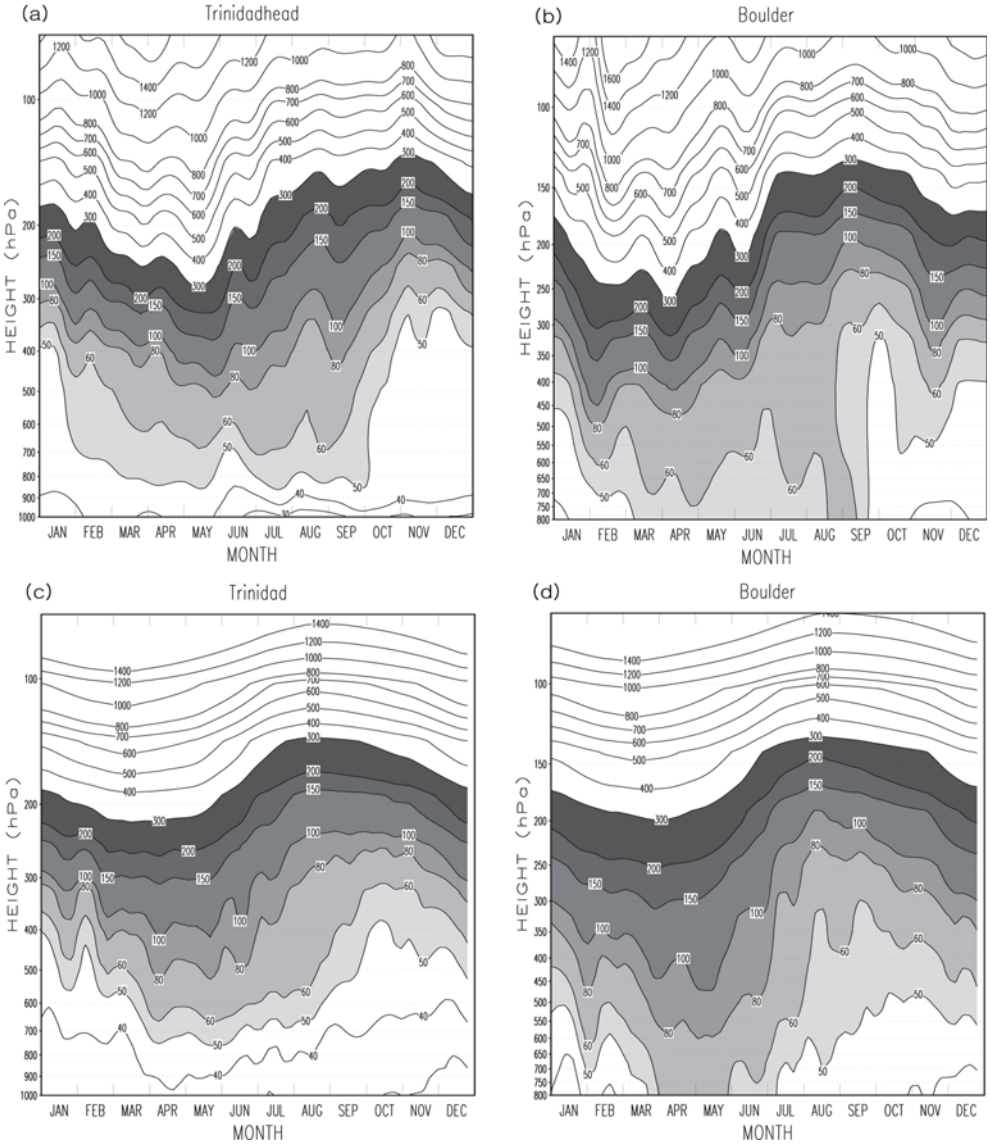


**Fig. 7.** Time-height cross sections of $O_3$ (ppbv) from measurements at Trinidadhead (41°N, 124°W) (a) and Boulder (40°N, 105°W) (b). The model calculation for these locations are shown in (c) and (d), respectively.

and long-range transport of continental anthropogenic pollutants are contributing factors to the northern hemisphere spring ozone maximum, the biomass burning emissions over the southeast Asia, Oceania, southern Africa, and South America regions, and transport of $O_3$ precursors such as PAN and NOx from soil and lightning (Schultz et al., 1999) are contributing factors for the southern hemisphere spring ozone maximum.

(5) Northern hemisphere high latitudes

Figure 7 extends the comparison of modeled $O_3$ vertical distribution with ozonesonde measurements to higher latitudes in the northern hemisphere. Both model and measurements at Trinidadhead and Boulder show high $O_3$ during spring in the lower stratosphere, and during the April-August period in the middle troposphere and near the surface. Limited ozonesonde measurements and model calculations at Fairbanks (not shown here) show similar timing for the occurrence of spring $O_3$ maximum compared with Trinidadhead and Boulder. Model calculations at the Azores (not shown here) also show elevated $O_3$ in the lower stratosphere in spring and in the middle troposphere during spring to summer seasons. These characteristics, high $O_3$ extending downward from the tropopause region, are close to the available measurements (Oltmans et al., 1996).

### *c. Effect of stratospheric $O_3$ on tropospheric $O_3$ distribution*

(1) Surface structure

For the southern hemisphere spring season, observational studies have shown surface $O_3$ maximum prevails over the

southern oceans (e.g., Fishman et al., 1986, 1991). The areas of elevated $O_3$ extends from the southern Atlantic, through southern Africa, to the Indian Ocean and extends beyond Australia to the south of eastern Pacific close to South America (Fig. 8b).

The areas of elevated $O_3$ over the southern hemisphere marine environment are dramatically replaced by $O_3$ with contours between 10 ppbv and 15 ppbv in the simulation without stratospheric $O_3$ (Fig. 8a). The magnitude and distribution of the $O_3$ ratios at the surface (shown as the $O_3$ ratios) ranges from close to 90% in the equator-ward latitudes to lower than 30% in the pole-ward latitudes (Fig. 8c). The reduction in ozone over the high latitudes is greater than those over the low latitudes. These calculations show that $O_3$ in the tropical latitudes, particularly over continents, are influenced more by photochemical processes in the troposphere than by the intrusion of $O_3$ from the stratosphere. In particular, over tropical continents, emissions of $O_3$ precursors from pronounced biomass burning are known as a dominant factor of the photochemical processes (e.g., Fishman et al., 1986, 1991; Browell et al., 1996; Diab et al., 1996; Jacob et al., 1996; Thompson et al., 1996).

Note that high $O_3$ ratios are seen over areas of intense biomass burning such as South America, central Africa, and southeast Asia, indicating that more than 80%-90% of $O_3$ in these regions are dominated by photochemically produced $O_3$ within the troposphere. Other areas showing high $O_3$ ratios are over the industrial regions such as the eastern U.S. ($\geq$ 80%), Europe ($\geq$ 70%), and east Asia ($\geq$ 60%), indicating that more than 60%-80% of surface $O_3$ are photochemically produced in the troposphere due to anthropogenic emissions of $O_3$ precursors such NOx, hydrocarbons and CO. The areas with large anthropogenic and biomass burning emissions can be readily identified in Fig. 8a, which shows high surface $O_3$ concentrations in these emission regions.

It is noteworthy that high $O_3$ ratios ($\geq$ 60%) appear in a narrow latitudinal band (centred around 10°N) over the tropical oceans of the Atlantic, the Indian, and the Pacific. The high $O_3$ ratios over these remote clean marine environments highlight the areas directly impacted from within the troposphere itself, namely by anthropogenic emissions and biomass burning emissions. For example, a large $O_3$ ratio of greater than 80% downwind but close to the Asian continent (the source of ozone precursors) and Southeast Asia (where biomass burning occurs) is predicted by the model. The $O_3$ ratios gradually reduce to 50-60% over the downwind areas such as the central (~70%) and eastern Pacific (~60%). The $O_3$ ratios over the equatorial Atlantic is greater than 70%.

For surface $O_3$ over the northern hemisphere spring season, the simulation without stratospheric $O_3$ shows elevated surface $O_3$ concentrations distributed over the continental emission source regions, and over the remote tropical marine boundary layer environments downwind from the continental emissions areas, such as the tropical Atlantic Ocean, the tropical Indian Ocean, and the tropical Pacific Ocean areas (Fig. 9a). Figure 9b shows mean surface $O_3$ distribution calculated with stratospheric $O_3$. The continental outflows over the marine boundary layer helps to maintain a weak global asymmetry in surface $O_3$ when comparing the northern hemisphere to the southern hemisphere oceanic environments. For latitudes outside the tropical regions, a dramatic reduction in $O_3$ to concentrations between 10 ppbv and 15 ppbv are calculated by the model without stratospheric $O_3$ (Fig. 9a).

The distribution of the $O_3$ ratios (Fig. 9c) shows a sharp reduction in surface $O_3$ to about 30%-40% of the original surface $O_3$ concentrations over the extra-tropical latitudes of the marine boundary layer when the model stratospheric $O_3$ is included. Continental regions such as the Amazon basin and South America, equatorial south Africa, southeast Asia, eastern U.S., Europe, and east Asia all exhibit high surface $O_3$ levels and high $O_3$ ratios even without stratospheric $O_3$ (Fig. 9a). This characteristic also appears in Fig. 8. These geographical areas are more influenced by the tropospheric photochemical processes than by $O_3$ from the stratosphere. For example, over the equatorial oceans of the Pacific, the Atlantic, and the Indian, high surface $O_3$ co-exist with the high $O_3$ ratios. These high $O_3$ ratios indicate that the tropical marine boundary layer is largely influenced by nearby continents rather than by the stratosphere.

The above results show that the surface $O_3$ over the continental regions (South America, south Africa, eastern U.S., Europe, southeast Asia, and east Asia) and over the tropical marine boundary layer are dominated by photochemical processes in the troposphere, with a minor contribution from the stratosphere. No distinctive inter-hemispheric asymmetry in spring over the extra-tropics of the marine boundary layer is shown in the calculation without stratospheric $O_3$. The maintenance of an inter-hemispheric asymmetry in spring over the extra-tropics marine boundary layer is largely driven by $O_3$ from the stratosphere, with in-situ photochemistry playing a minor role.

(2) Zonal-mean structure

Figure 10 compares the zonal mean cross-section of the $O_3$ ratios for four different seasons. In boreal summer, June-August (Fig. 10b), more than 60% of $O_3$ in the northern hemisphere lower troposphere (below 700 hPa) is produced as a result of tropospheric photochemistry. This magnitude reduces with height, to less than 10%-20% close to the tropopause. On the contrary, only about 20%-40% of $O_3$ is produced in the southern hemisphere lower troposphere during this period. There is a greater contribution from tropospheric photochemistry to the free troposphere in the northern hemisphere (~20%-60%) than in the southern hemisphere during the season (~10%-20%), indicating that $O_3$ from the surface photochemistry affects the free troposphere more efficiently in the summer hemisphere where the lower troposphere is basically behaving like a photochemical source of $O_3$.

A similar behavior is found when the season moves to the austral summer (Fig. 10d). For example, more than 40%-50% of $O_3$ is photochemically produced in the southern hemisphere

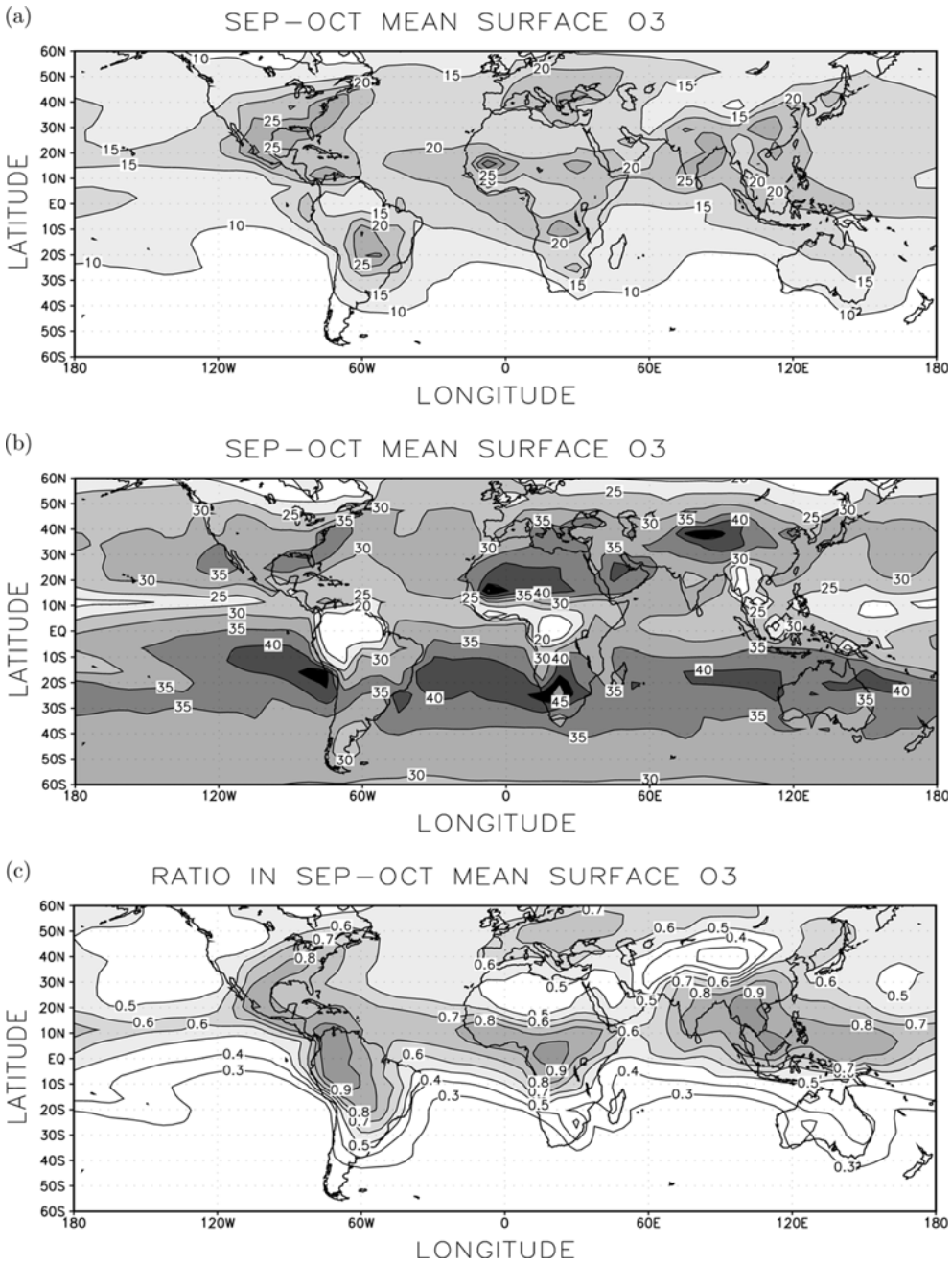


**Fig. 8.** September to October mean ozone distributions (ppbv) calculated at the surface for (a) without and (b) with stratospheric $O_3$, and (c) the ratio between the calculations without to that with stratospheric $O_3$ in the model.

lower troposphere. A large $O_3$ ratio in the southern hemisphere than in the northern hemisphere free troposphere indicates more photochemical ozone production in the summer southern hemisphere than in the winter northern hemisphere. A significant difference between the northern hemisphere and the southern hemisphere summer season is that more than 70% of zonal mean $O_3$ is produced close to the surface in the northern hemisphere whereas only about 50% in the southern hemisphere, consistent with more intensive emissions of precursors in the northern hemisphere.

During the two spring seasons, both March-May (Fig. 10a) in the northern hemisphere and September-November (Fig. 10c) in the southern hemisphere, the contribution from tropospheric photochemistry in the lower troposphere is significantly reduced to less than 20% to 50% for latitudes outside the tropical region. There is slightly larger $O_3$ ratio in the northern hemisphere during September-November than in the southern hemisphere during March-May, possibly indicating more residual $O_3$ from the previous summer season in the northern hemisphere than in the southern hemisphere. For the tropical

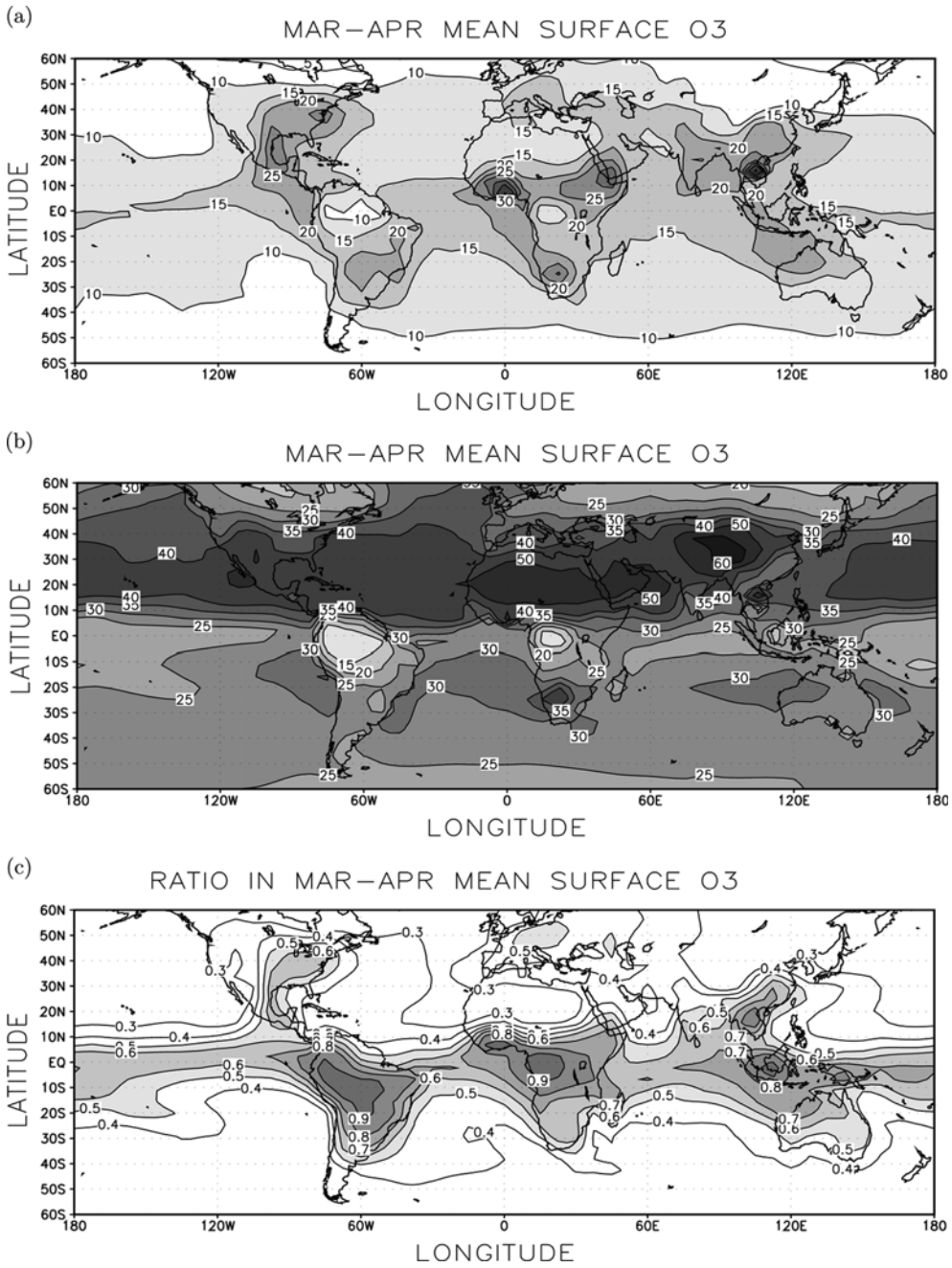


**Fig. 9.** The same as in Figure 8 but for March to April.

troposphere, a $O_3$ ratio greater than 50% indicates that both the tropospheric photochemistry and effect of convective transport (or large-scale transport by Hadley circulation) are major contributors in this part of the atmosphere. The northern hemisphere shows no signs of spring $O_3$ maximum in the calculation without stratospheric $O_3$.

By using a stratospheric $O_3$ tracer, Roelofs et al. (1997) estimated that $O_3$ transported from the stratosphere is about the same to that of photochemically produced in the troposphere. Wang et al. (1998) estimated that photochemical production of $O_3$ in the upper, middle, and continental lower troposphere contribute to 10% to 50% of $O_3$ concentrations in the troposphere.

### *d. Comparing model ozone profiles*

(1) The Atlantic Basin

Figure 11 compares time-height cross sections of modeled $O_3$ at two tropical Atlantic stations in the Northern Hemisphere (Bermuda) and Southern Hemisphere (Ascension Island). The hemispheric spring ozone maximum is shown in the measurements (Fig. 2), and the model calculation with stratospheric $O_3$

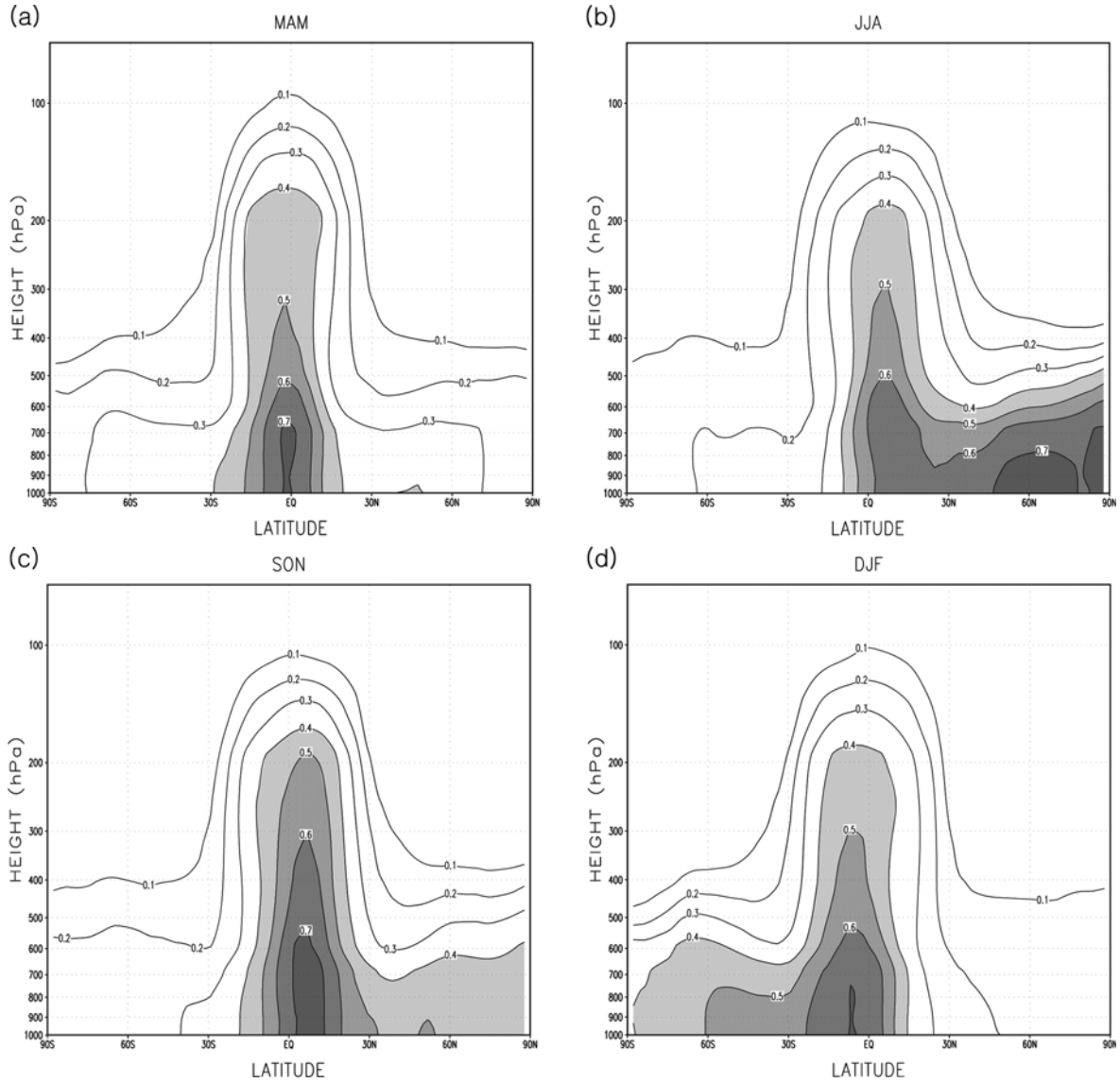


**Fig. 10.** Zonal average of the $O_3$ ratios for (a) March, April, and May, (b) June, July, and August, (c) September, October, and November, (d) December, January, and February.

can reproduce this feature at these two sites (shown in a separate work). For the calculation without $O_3$ from the stratosphere, distinctive ozone maxima appear in the middle to lower troposphere during spring to summer at Bermuda (Fig. 11a). At Ascension Island (Fig. 11b), elevated $O_3$ appears in the middle to the upper troposphere during the southern hemisphere spring to late summer. Time-series distributions of the $O_3$ ratios (Figs. 11c, d) show that more than 60%-70% of $O_3$ in the lower troposphere during spring and summer is photochemically produced. This result is consistent with other studies (most of them based on trajectory analyses) which showed that transport of photochemically produced $O_3$ due to biomass burning emissions and $O_3$ producing precursors from continents is the major factor for high $O_3$ observed in the lower troposphere at these sites (e.g., Moody et al., 1995; Browell et al., 1996; Diab et al., 1996; Jacob et al., 1996; Logan, 1998; Oltmans et al., 1996; Thompson et al., 1996).

We also compare $O_3$ profiles from ozonesondes with model calculations at two sub-tropical locations (La Reunion (21°S, 56°E) and Irene (26°S, 28°E)) over the southern hemisphere western Indian Ocean (not shown here). The measurements at these sites show the southern hemisphere spring $O_3$ maximum throughout the troposphere, while the calculations without stratospheric $O_3$ also shows the southern hemisphere spring $O_3$ maximum at these sites, with tropospheric photochemistry produce more than 50-70% of $O_3$ in the lower troposphere during the southern hemisphere late winter to spring. Our model simulations concur with previous studies which concluded that tropospheric photochemistry, derived from biomass burning emissions is the major factor for $O_3$ in this region (e.g., Baldy et al., 1996; Diab et al., 1996). For example, Baldy et al. (1996) reported that the elevated $O_3$ in the free troposphere

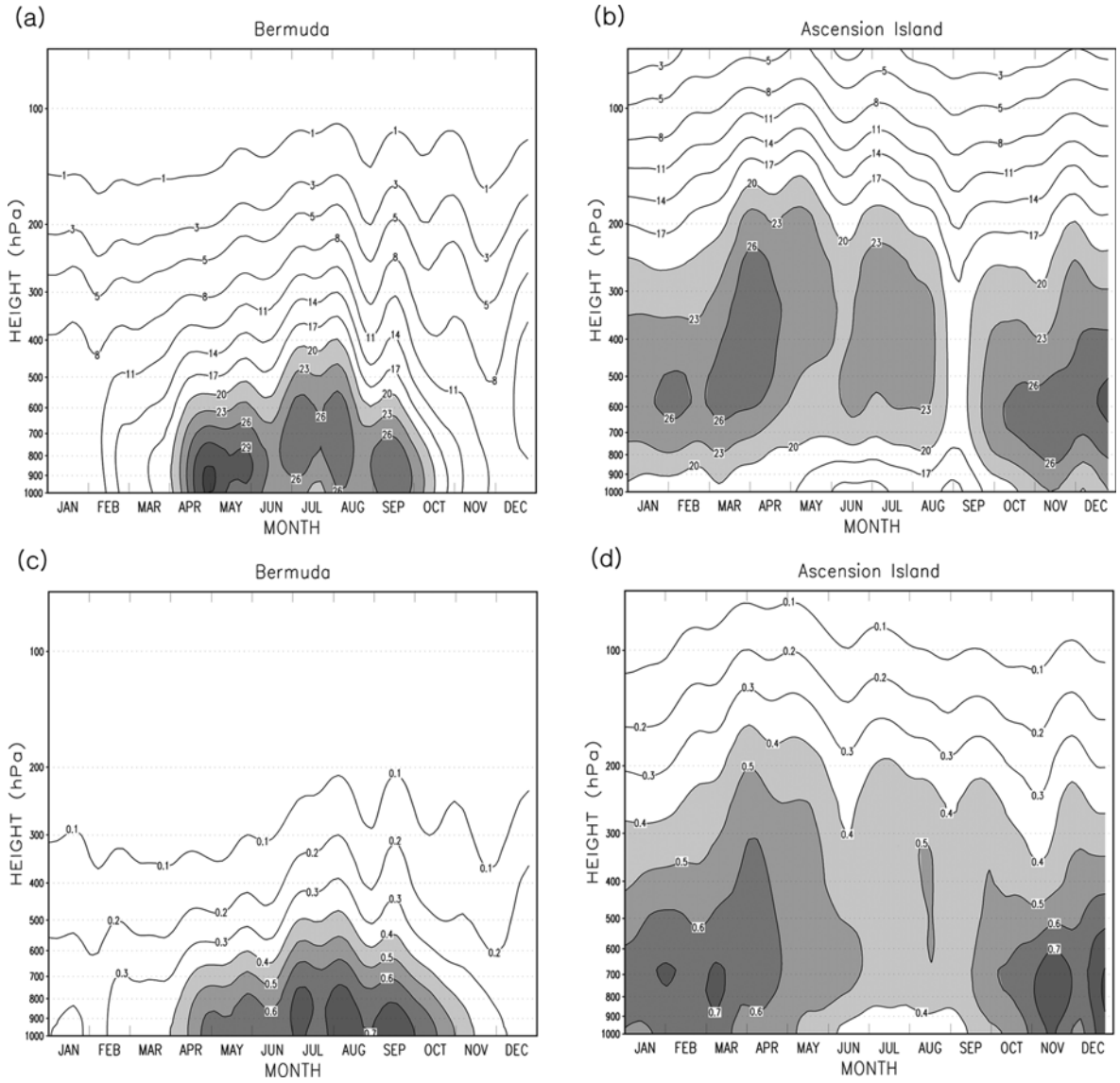


**Fig. 11.** Time-height cross sections of $O_3$ (ppbv) from model calculation without stratospheric $O_3$ at Bermuda (32°N, 65°W) (a) and Ascension Island (8°S, 14.4°W) (b); (c) and (d) show ratio of $O_3$ calculated without to that with stratospheric $O_3$ in the model.

during this period of time at this island (Le Reunion) is concomitant with active biomass burning in the southeastern African continent and Madagascar, and Thompson et al. (1996) reported that features of elevated tropospheric $O_3$ (≥ 90 ppbv) extend over the southeast Indian Ocean, Africa, the Atlantic, and eastern South America during September-October.

(2) The Pacific Basin

Figure 12 compares time-height sections of vertical $O_3$ profiles from model calculations at Taiwan (in the subtropical western North Pacific), and Tahiti (in the central-east South Pacific). Observed $O_3$ profiles at Taiwan shows a similar spring ozone maximum in the troposphere as to that for Bermuda in the northern Atlantic, and Hawaii in the eastern North Pacific (not shown). The model with stratospheric $O_3$ shows a similar spring ozone maximum as the measurements, although the elevated ozone concentrations do not extend to low altitude (below 600 hPa) as in the measurements. The major differences at altitudes below 4 km (~600 hPa) coincide with the altitude range most influenced by continental outflow (e.g., Crawford et al., 1997; Kajii et al., 1997). This continental effect is clearly indicated in the model calculation without $O_3$ from the stratosphere (Fig. 12a). Two pronounced $O_3$ maxima were calculated at Taiwan, one during the northern hemisphere spring, and the other one during the northern hemisphere summer. While the summer maximum is associated with strong photochemical production, transport from the Asian continent plays a key role in the spring maximum in this region. As shown in the distribution of the $O_3$ ratios (Fig. 12c), more than 60%-70% of photochemically produced $O_3$ is limited to the lower tropo-

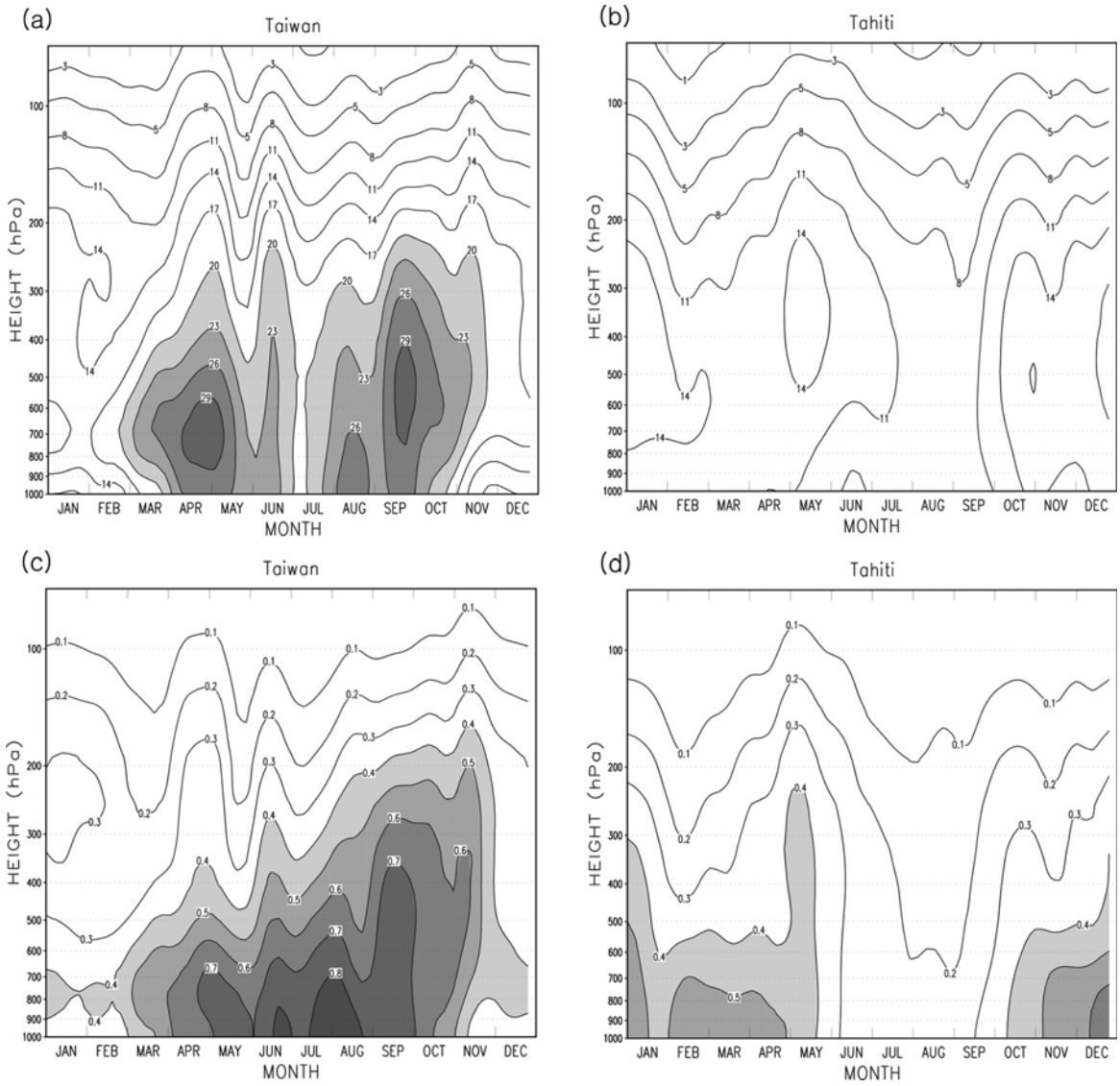


**Fig. 12.** The same as in Figure 11 but for Taiwan (25°N, 121°E) and Tahiti (18°S, 150°W), respectively.

sphere in spring, while more than 70%-80% $O_3$ can be photochemically produced from the surface to higher altitudes (close to 400 hPa) in summer. Wang et al. (1998) argued that the spring $O_3$ maximum at Hawaii is due to long-rang transport of Asian pollution. Based on back trajectory analyses, Perry et al. (1999) concluded that the observed spring maximum in aerosol at Mauna Loa is due to long-range transport from Asia and North America continents.

The South Pacific is the region of the tropical troposphere most remote from human activity (Schultz et al., 1999). At Tahiti, a pronounced southern hemisphere spring ozone maximum is seen in the troposphere. It has been argued that the timing of this southern hemisphere spring $O_3$ maximum coincides with the intensive southern hemisphere biomass burning activities take place in South America, Africa, Southeast Asia, and Oceania (Schultz et al., 1999). This southern hemisphere spring $O_3$ maximum is shown in the calculation without stratospheric $O_3$ in the model (Fig. 12b). About 40%-60% of $O_3$ in the lower troposphere during this period is associated with photochemical production, which can last into the southern hemisphere autumn.

(3) Northern high latitudes

Figure 13 examines the effects of stratospheric $O_3$ at high latitude locations. For the calculation without stratospheric $O_3$, the model produces a summer maximum (Figs. 13a, b), and about 50%-80% of $O_3$ in the lower troposphere at these sites are photochemically produced during the northern hemisphere summer. About 20%-40% is due to tropospheric photochemistry in the lower troposphere during the northern hemisphere spring. About 10%-20% is photochemically produced for higher altitudes. Hence, $O_3$ from the stratosphere is the dominating factor for the spring $O_3$ maximum at these locations.

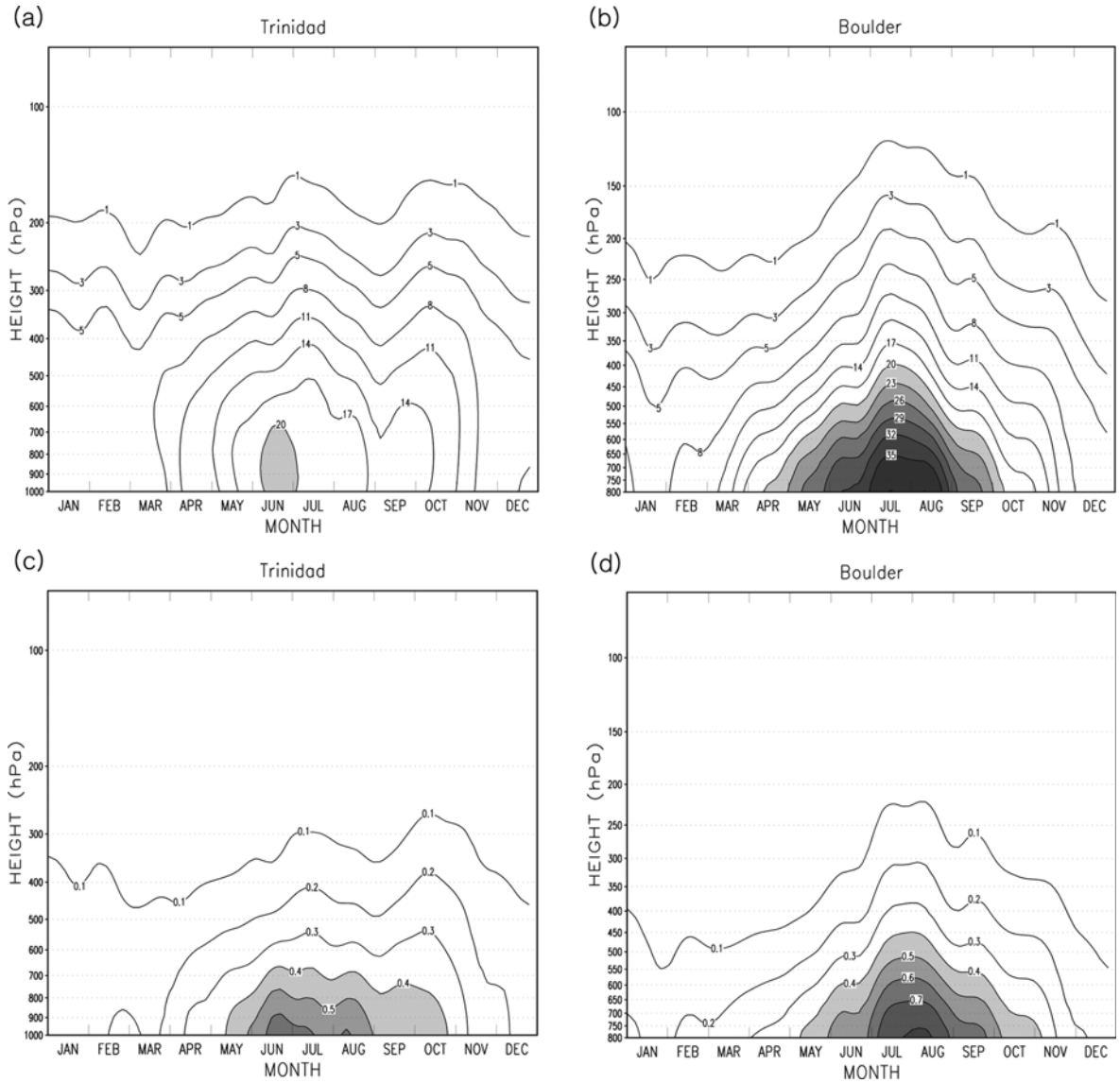


**Fig. 13.** The same as in Fig. 11 but for Trinidad Head (41.1°N, 124.2°W) and Boulder (40°N, 105°W), respectively.

## 4. Summary

In this work we examine the effect of $O_3$ from the stratosphere on the $O_3$ levels in the troposphere. The tropopause is defined according to the PV and potential temperature distribution. An annual simulation is performed without $O_3$ in the model, and the results were compared with the previous simulation which includes $O_3$ in the stratosphere.

Our results show that surface $O_3$ over the tropical marine boundary layer are dominated by in-situ photochemical production, while transport of $O_3$ from the stratosphere plays a minor role. However, the inter-hemispheric asymmetry in $O_3$ in the extra-tropics marine boundary layer is driven mainly by the transport of $O_3$ from the stratosphere, while in-situ photochemistry plays a minor role.

Comparison with surface measurements show that the calculation with stratospheric $O_3$ can reproduce the observed spring $O_3$ maximum at the surface, while the calculation without $O_3$ from the stratosphere shows no clear indication of a hemispheric spring maximum. Instead, the calculation without stratospheric $O_3$ shows a hemispheric summer maximum, indicating the important contribution of transport of $O_3$ and $O_3$ producing precursors from continental regions during the summer months. Time-series distributions of the $O_3$ ratios show that more than 60%-70% of $O_3$ in the lower troposphere in the tropical Atlantic basin during spring is photochemically produced. Tropospheric photochemistry driven by biomass burning emissions is the major factor for $O_3$ in the eastern Indian Oceanand southern Africa regions.

In the tropical western North Pacific Ocean, in-situ photochemistry contributes 60%-70% of $O_3$ in spring in the lower troposphere, while 70-80% of $O_3$ is photochemically produced

in summer. In the tropical south Pacific, the model shows that about 40%-90% of $O_3$ in the lower troposphere is photochemically produced from spring to late winter at Fiji and Tahiti. In the northern hemisphere mid-latitude, about 50-80% of $O_3$ in the lower troposphere are photochemically produced during the northern hemisphere summer season. About 20%-40% is due to tropospheric photochemistry in the lower troposphere during the northern hemisphere spring season. About 10%-20% is photochemically produced for higher altitudes. Hence, the $O_3$ from stratosphere is the dominating factor for the spring $O_3$ maximum in the northern hemisphere mid-latitude.

***Acknowledgments.*** We are very grateful to the BADC, ECMWF, NASA SHADOZ project, S. J. Oltmans of ESRL/NOAA, and Central Weather Bureau for the data. We thank D. E. Shallcross and J. A. Pyle for support on this work. We are very grateful to two anonymous reviewers for their insightful comments that significantly increase the clarity of this paper. This research was supported by the NSC grant NSC-89-2119-M-008-007.

**Edited by:** Rokjin Park

## REFERENCES

Baldy, S., G. Ancellet, M. Bessafi, A. Badr, and D. Lan Sun Luk, 1996: Field observations of the vertical distribution of tropospheric ozone at the island of Reunion (southern tropics). *J. Geophys. Res.*, **101**, No. D19, 23,835-23,849.

Berntsen, T. K., and I. S. A. Isaksen, 1997: A global three-dimensional chemical transport model for the troposphere. 1. Model description and CO and ozone results. *J. Geophys. Res.*, **102**, No. D17, 21239-21280.

Bethan, S., G. Vaughan, S. J. Reid, 1996: A comparison of ozone and thermal tropopause heights and the impact of tropopause definition on quantifying the ozone content of the troposphere. *Quart. J. Roy. Meteor. Soc.*, **122**, 929-944.

Browell, E. V., and Coauthors, 1996: Ozone and aerosol distributions and air mass characteristics over the South Atlantic Basin during the burning season. *J. Geophys. Res.*, **101**, 24,043-24,068.

Crawford, J., and Coauthors, 1997: As assessment of ozone photochemistry in the extratropical western North Pacific: Impact of continental outflow during the late winter/early spring. *J. Geophys. Res.*, **102**, No. D23, 28,469-28,487.

Diab, R. D., and Coauthors, 1996. Vertical ozone distribution over southern Africa and adjacent oceans during SAFARI-92. *J. Geophys. Res.*, **101**, No. D19, 23,823-23,833.

Elbern, H., J. Hendricks, and A. Ebel, 1998: A climatology of tropopause folds by global analyses. *Theor. Appl. Climatol.*, **59**, 181-200.

Fishman, J., P. Minnis, H. G. Reichle Jr., 1986: The use of satellite data to study tropospheric ozone in the tropics. *J. Geophys. Res.*, **91**, 14,451-14,465.

_____, K. Fakhruzzaman, B. Cros, and D. Nganga, 1991: Identification of widespread pollution in the Southern Hemisphere deduced from satellite analyses. *Science*, **252**, 1693-1696.

Hack, J. J., B. A. Boville, B. P. Briegleb, J. T. Kiehl, P. J. Rasch, D. L. Williamson, 1993: Description of the NCAR Community Climate Model (CCM2). *NCAR Technical Note*, *NCAR/TN-382+STR*, National Center for Atmospheric Research, Boulder, Colorado.

Hess, P. G., and R. Zbinden, 2013: Stratospheric impact on tropospheric ozone variability and trends: 1990-2009. *Atmos. Chem. Phys.*, **13**, 649-674.

Holton, J. R., P. H. Haynes, M. E. McIntyre, A. R. Douglass, R. B. Rood, and L. Pfister, 1995: Stratosphere-troposphere exchange. *Rev. Geophys.*, **33**, 403-439.

Hoskins, B. J., 1991: Towards a PV-θ view of the general circulation. *Tellus*, **43AB**, 27-35.

Hsu, J., and M. J. Prather, 2009: Stratospheric variability and tropospheric ozone. *J. Geophys. Res.*, **114**, D06102, doi:10.1029/2008JD010942.

Jacob, D. J., and Coauthors, 1996: Origin of ozone and NOx in the tropical troposphere: A photochemical analysis of aircraft observations over the South Atlantic basic. *J. Geophys. Res.*, **101**, 24,235-24,250.

Jaffe, D., A. Mahura, J. Kelly, J. Atkins, P. C. Novelli, and J. Merrill, 1997: Impact of Asian emissions on the remote North Pacific atmosphere: Interpretation of CO data from Shemya, Guam, Midway and Mauna Loa. *J. Geophys. Res.*, **102**, 28,627-28,635.

Kajii, Y., H. Akimoto, Y. Komazaki, S. Tanaka, H. Mukai, K. Murano, and J. T. Merrill, 1997: Long-range transport of ozone, carbon monoxide, and acidic trace gases at Oki Island, Japan, during PEM-West B / PEACAMPOT B campaign. *J. Geophys. Res.*, **102**, 28,637-28,649.

Künzli, N., and Coauthors, 2000: Public-health impact of outdoor and traffic-related air polution: a European assessment. *Lancet*, **356**, 795-801.

Lelieveld, J., and F. J. Dentener, 2000: What controls tropospheric ozone?. *J. Geophys. Res.*, **105**, No. D3, 3531-3551.

Logan, J. A., 1999a: An analysis of ozonesonde data for the troposphere: Recommendations for testing 3-D models and development of a gridded climatology for tropospheric ozone. *J. Geophys. Res.*, **104**, No. D13, 16,115-16,149.

_____, 1999b. An analysis of ozonesonde data for the lower stratosphere: Recommendations for testing models. *J. Geophys. Res.*, **104**, No. D13, 16,151-16,170.

Monks, P. S., 2000: A review of the observations and origins of the spring ozone maximum. *Atmos. Environ.*, **34**, 3545-3561.

Moody, J. L., S. L. Oltmans, H. Levy II, and J. T. Merrill, 1995: Transport climatology of tropospheric ozone: Bermuda, 1988-1991. *J. Geophys. Res.*, **100**, 7179-7194.

Neu, J. L., T. Flury, G. L. Manny, M. L. Santee, N. J. Livesey, and J. Worden, 2014. Tropospheric ozone variations governed by changes in stratospheric circulation. *Nat. Geosci.*, **7**, 340-344.

Oltmans, S. J., and Coauthors, 1996. Summer and spring ozone profiles over the Atlantic from ozonesonde measurements. *J. Geophys. Res.*, **101**, 29,179-29,200.

Perry, K. D., T. A. Cahill, R. C. Schnell, and J. M. Harris, 1999: Long-range transport of anthropogenic aerosols to the National Oceanic and Atmospheric Administration baseline station at Mauna Loa Observatory, Hawaii. *J. Geophys. Res.*, **104**, No. D15, 18,521-18,533.

Roelofs, G.-J., and J. Lelieveld, 1997: Model study of the influence of cross-tropopause $O_3$ transport on the tropospheric $O_3$ levels. *Tellus*, **49B**, 38-55.

_____, _____, and R. van Dorland, 1997: A three-dimensional chemistry/general circulation model simulation of anthropogenically derived ozone in the troposphere and its radiative climate forcing. *J. Geophys. Res.*, **102**, No. D19, 23,389-23,401.

Rokjin J. Park, and Sang-Woo Kim, 2014: Air Quality Modeling in East Asia: Present Issues and Future Directions. *Asia-Pac. J. Atmos. Sci.*, **50**, 105-120.

Schauffler, S. M., and J. S. Daniel, 1994: On the effects of stratospheric circulation changes on trace gas trends. *J. Geophys. Res.*, **99**, No. D12, 25,747-25,754.

Schultz, M. G., and Coauthors, 1999: On the origin of tropospheric ozone and NOx over the tropical South Pacific. *J. Geophys. Res.*, **104**, 5829-

5843.

Thompson, A. M., K. E. Pickering, D. P. McNamara, M. R. Schoeberl, R. D. Hudson, J. H. Kim, E. V. Browell, V. W. J. H. Kirchhoff, and D. Nganga, 1996: Where did tropospheric ozone over southern Africa and the tropical Atlantic come from in October 1992? Insights from TOMS, GTE TRACE A, and SAFARI 1992. *J. Geophys. Res.*, **101**, 24,251-24,278.

Tourre, Y. M., and W. B. White, 2005: Evolution of the ENSO signal over the tropical Pacific-Atlantic domain. *Geophys. Res. Lett.*, **32**, L07605, doi:10.1029/2004GL022128.

Vaughan, G., J. D. Price, and A. Howells, 1994: Transport into the troposphere in a tropopause fold. *Quart. J. Roy. Meteor. Soc.*, **120**, 1085-1103.

Voulgarakis, A., P. Hadjinicolaou, J. A. Pyle, 2011: Increases in global tropospheric ozone following an El Niño event: examining stratospheric ozone variability as a potential driver. *Atmos. Sci. Lett.*, **12**, 228-232.

Wang, K.-Y., J. A. Pyle, and D. E. Shallcross, 2001a: Formulation and evaluation of IMS, an interactive three-dimensional tropospheric chemical transport model 1. Model emission schemes and transport processes. *J. Atmos. Chem.*, **38**, 195-227.

_____, _____, D. E. Shallcross, and D. J. Lary, 2001b: Formulation and evaluation of IMS, an interactive three-dimensional tropospheric chemical transport model 2. Model chemistry and comparison of modelled $CH_4$, CO, and $O_3$ with surface measurements. *J. Atmos. Chem.*, **38**, 31-71.

Wang, Y., J. A. Logan, and D. J. Jacob, 1998: Global simulation of tropospheric $O_3$-$NO_x$-hydrocarbon chemistry 3. Origin of tropospheric ozone and effects of nomenthane hydrocarbons. *J. Geophys. Res.*, **103**, 10,757-10,767.